Lattice Dynamics of Beryllium*

R. E. SCHMUNK, R. M. BRUGGER, P. D. RANDOLPH, AND K. A. STRONG
Atomic Energy Division, Phillips Petroleum Company, Idaho Falls, Idaho

(Received June 7, 1962)

Measurements of the dispersion relations for waves propagating in the [0001] and [01$\bar{1}$0] directions in beryllium have been made using the MTR phased-chopper slow-neutron velocity selector. In the [01$\bar{1}$0] direction only one of the transverse modes was available for investigation, that having atom displacement normal to the basal plane. Two distinct frequencies were observed at the center of the Brillouin zone for the optical branches, and the corresponding branches are referred to as upper optical and lower optical. For both symmetry directions, the upper optical branch corresponds to the mode of vibration having the polarization vector parallel to the hexagonal axis. Pertinent frequencies in units of 10^{13} sec^{-1} are: (at the center of the zone) upper optical, 1.99 ± 0.07; lower optical, 1.33 ± 0.04; (at the zone boundary in the [0001] direction) lower optical and transverse acoustical, 1.01 ± 0.06; upper optical and longitudinal acoustical, 1.57 ± 0.07; (at the zone boundary in the [01$\bar{1}$0] direction) upper optical, 1.69 ± 0.09; lower optical, 1.63 ± 0.08; longitudinal acoustical, 1.54 ± 0.08; transverse acoustical, 1.21 ± 0.05. The mode of vibration for a particular phonon was determined from the region of reciprocal space in which the transition was observed. The initial slopes of the acoustical branches agree well with elastic constant data, except for the longitudinal branch in the [0001] direction. Lattice dynamics models of Begbie and Born and of Slutsky and Garland, the latter extended to include interactions with fourth and fifth nearest neighbors, give limited agreement with the present data only when the force constants in the models are evaluated from the neutron-scattering data.

I. INTRODUCTION

USING the MTR phased-chopper slow-neutron velocity selector,[1] extensive measurements of the normal modes of vibration of beryllium (hexagonal close-packed structure) were made for waves traveling in the [0001] and [01$\bar{1}$0] directions. These data are compared with dispersion relations calculated from the model of Begbie and Born[2] and from the model of Slutsky and Garland.[3] Neither model is completely successful in explaining the data.

The dispersion relation for phonons in a crystal can be determined by measurements of the momentum changes and the energy changes occurring when slow neutrons are inelastically scattered from a single crystal. Previous examinations have been devoted mainly to the study of cubic crystal structures such as aluminum,[4–7] sodium,[8] sodium iodide,[9] germanium,[10] silicon,[11,12] and lead.[13] Preliminary data have been reported also for bismuth[14] and pyrolytic graphite,[15] which have the rhombohedral and graphite structures, respectively.

The dispersion relation of beryllium is a new contribution to the knowledge of solid-state physics because it represents a crystal symmetry class (hexagonal close packed) which has not been investigated extensively heretofore. Since beryllium has two atoms per primitive unit cell, the dispersion relation will have six branches: one longitudinal acoustical and two transverse acoustical branches and one longitudinal optical and two transverse optical branches. The optical branches do not have just one intercept at the center of the Brillouin zone as do monatomic cubic structures but two distinct intercepts. Because of the small atomic spacing in beryllium crystals and the comparatively large frequency range of their vibration spectrum, the study of the dispersion relation by neutron scattering is attainable with the present velocity selector resolution. In addition beryllium has a low neutron absorption cross section; it is a good coherent neutron scatterer, and a large single crystal of beryllium was immediately available for the experiment.

The scattering of slow neutrons by a material can be completely described by the nuclear scattering lengths and the solid state properties (symmetry class, dispersion relations, and structure factors). The scattering lengths[16] and the symmetry class[17] of beryllium are well known, and the structure factor can be approximated on the basis of lattice dynamics models. Thus the measurement of the dispersion relation is an important contribution for describing the scattering of slow

* Supported by the U. S. Atomic Energy Commission.

[1] R. M. Brugger and J. E. Evans, Nuclear Instr. and Methods **12**, 75 (1961).
[2] G. H. Begbie and M. Born, Proc. Roy. Soc. (London) **A188**, 179–208 (1946).
[3] L. J. Slutsky and C. W. Garland, J. Chem. Phys. **26**, 787 (1957).
[4] B. N. Brockhouse and A. T Stewart, Revs. Modern Phys. **30**, 236 (1958).
[5] R. S. Carter, H. Palevsky, and D. J. Hughes, Phys. Rev. **106**, 1168 (1957).
[6] K. E. Larson, U. Dahlborg, and S. Holmryd, Arkiv Fysik **17**, 369–392 (1960).
[7] J. L. Yarnell, J. L. Warren, and S. H. Koenig, Bull. Am. Phys. Soc. **7**, 343 (1962).
[8] A. D. B. Woods, B. N. Brockhouse, R. H. March, and R. Bowers, Bull. Am. Phys. Soc. **6**, 261 (1961).
[9] A. D. B. Woods, W. Cochran, and B. N. Brockhouse, Phys. Rev. **119**, 980 (1960).
[10] B. N. Brockhouse and P. K. Iyengar, Phys. Rev. **111**, 747 (1958).
[11] B. N. Brockhouse, Phys. Rev. Letters **2**, 256 (1959).
[12] H. Palevsky, D. J. Hughes, W. Kley, and E. Tunkelo, Phys. Rev. Letters **2**, 258 (1959).
[13] B. N. Brockhouse, G. Caglioti, M. Sakamoto, R. N. Sinclair, and A. D. B. Woods, Bull. Am. Phys. Soc. **5**, 39 (1960).
[14] S. H. Koenig and J. Yarnell, Bull. Am. Phys. Soc. **5**, 198 (1960).
[15] G. Dolling and B. N. Brockhouse, Bull. Am. Phys. Soc. **7**, 17 (1962).
[16] G. E. Bacon, *Neutron Diffraction* (Clarendon Press, Oxford, 1955).
[17] W. B. Pearson, *A Handbook of Lattice Spacings and Structures of Metals and Alloys* (Pergamon Press, New York, 1958).

neutrons by beryllium. Since beryllium is an important reactor moderator and reflector, these descriptions are important in understanding the moderation, thermalization, and space distribution of the fluxes in a beryllium reactor assembly.

Measurements of the dispersion relations $\nu=\nu(\mathbf{q})$ by neutron spectrometry are interpreted through the energy and momentum conservation relations[10]:

$$\Delta E=E-E_0=h\nu,$$
and
$$\mathbf{Q}=\mathbf{k}_0-\mathbf{k}'=2\pi\boldsymbol{\tau}-\mathbf{q}. \tag{1}$$

Here, E, E_0, and ΔE are the final and initial neutron energies and the energy change, respectively; ν is the phonon frequency, a function of the phonon wave vector $\mathbf{q}$; $\mathbf{k}_0$ and $\mathbf{k}'$ are the initial and final neutron wave vectors, respectively; $\boldsymbol{\tau}$ is a translation vector of the reciprocal lattice. In the experiment, the initial neutron energy E_0 and the crystal orientation relative to the incident neutrons (or the orientation of $\mathbf{k}_0$ relative to the crystal lattice) were variable parameters. From a given peak in the coherent inelastic neutron scattering data, one determines E and k', and hence, a single point in the dispersion relation $\nu=\nu(\mathbf{q})$ is obtained. By making many measurements with different initial energies and different orientations of the crystal, the complete dispersion relation for all directions in the crystal can be determined.

In mapping the $\nu(\mathbf{q})$ relation from neutron scattering data, it is important to maximize the cross section for neutron-phonon interactions which one wishes to observe and at the same time to remove competing effects as much as possible. To this end it is necessary to consider the differential cross section for one-phonon coherent scattering. This relation has been given as[10]

$$\sigma_j(\mathbf{k}_0\rightarrow\mathbf{k}')=\frac{\hbar}{4\pi}\frac{k'}{k_0}\begin{Bmatrix}N_j\\N_j+1\end{Bmatrix}e^{-2w}\frac{g_j^2}{J_j}, \tag{2}$$

per unit cell steradian for neutrons interacting with the jth phonon branch. The quantity $N_j=[\exp(h\nu/k_BT)-1]^{-1}$ applies for neutron energy gain, while N_j+1 applies for neutron energy loss; e^{-2w} is the Debye-Waller factor and $J_j=1+(\epsilon h/2E')[\mathbf{k}'\cdot\mathrm{grad}_q\nu_j]$, where $\epsilon=+1$ for neutron energy gain, $\epsilon=-1$ for neutron energy loss, and h is Planck's constant. The factor g_j^2, analogous to the structure factor of x-ray scattering, takes into consideration the dynamics of the atomic motions. The factor g_j^2 was calculated for beryllium and applied in the scattering measurements which were made. The calculation of g_j^2 is presented in Sec. II.

In this experiment the optical branches are referred to as upper optical (UO) and lower optical (LO), and the acoustical branches are referred to as transverse (TA) and longitudinal (LA). This identification avoids confusion which might arise if the conventional identification was followed (e.g., the upper optical branch in the [0001] direction would be identified as longitudinal optical while the upper optical branch in the $[01\bar{1}0]$ direction would be identified as transverse optical). The optical frequencies at the center of the Brillouin zone are 1.99 ± 0.07 and 1.33 ± 0.04, both in units of 10^{13} sec^{-1}, for the upper and lower optical branches, respectively. For the [0001] direction the optical frequencies decrease for increasing value of the phonon wave vector and join the acoustical branches at the zone boundary at frequencies of 1.57 ± 0.07 (UO and LA) and 1.01 ± 0.06 (LO and TA), both in units of 10^{13} sec^{-1}. At a value of $q/q_{\max}\simeq0.6$, in the [0001] direction, the LO and LA branches intersect. Data obtained for the acoustical branches join smoothly to the initial slopes predicted from elastic constant data, and these branches display the usual decreasing slope for increasing wave vector, except for the LA[0001] branch where the neutron scattering data plot above the initial slope line for over half the wave vector range in the Brillouin zone. The Debye approximation appears reasonable for the acoustical branches in the [0001] direction but not for the $[01\bar{1}0]$ direction where the acoustical data deviate from a straight line by more than 10% at a wave vector value of $q/q_{\max}\simeq0.4$. Values for the $[01\bar{1}0]$ zone boundary intercepts are, all in units of 10^{13} sec^{-1}: UO, 1.69 ± 0.09; LO, 1.63 ± 0.08; LA, 1.54 ± 0.08; TA, 1.21 ± 0.05.

Lattice dynamics models which have been compared with the data of this experiment are due to Slutsky and Garland, hereafter referred to as SG, and Begbie and Born, hereafter referred to as BB. The SG model assumes simplified central-force interactions with nearest neighbors in the hexagonal plane and in addition nearest and next-nearest neighbors out of the hexagonal plane. In contrast, for the BB model no assumptions are made regarding the nature of the forces, and interactions are assumed with only nearest neighbors in and out of the hexagonal plane. The assumptions of the SG model requires 3 force constants while the more general BB model requires 8 constants. In both models the microscopic force constants are related to the five elastic constants for hexagonal crystals. Experimental values of the elastic constants of beryllium, reported by Smith and Arbogast,[18] permit the evaluation of five of the eight force constants in the BB model and all of the constants in the SG model. By introducing these values of the force constants into the dynamic equations one can compare the models directly with the experimental data. With the force constants evaluated in this way, neither model matches the data, particularly in the predicted optical frequencies which are as much as 25% higher than the observed values.

Since for certain values of the phonon wave vector, the dynamic equations simplify yielding the frequency squared as a linear combination of the force constants, it is also possible to evaluate the force constants

[18] J. F. Smith and C. L. Arbogast, J. Appl. Phys. **31**, 99 (1960).

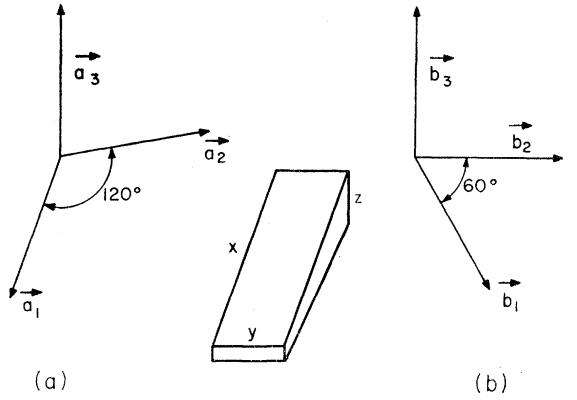

FIG. 1. Basis translation vectors of (a) the direct lattice and (b) the reciprocal lattice of beryllium, showing their orientation relative to the single-crystal sample. Sample dimensions are $x=7$ in., $y=1.72$ in., and $z=1.08$ to 0.47 in.

directly in terms of the neutron scattering data. Values of the force constants arrived at in this way and used in the dynamic equations give improved, although still limited, agreement between the models and experiment. The SG model was extended to include interactions with fourth and fifth nearest neighbors, and the general results of this calculation are given in the Appendix. The extended SG model, with the constants evaluated from the neutron data, is compared with experiment, and it is concluded that agreement is sufficiently good so that the model can be used to calculate a frequency distribution for beryllium, and for preliminary reactor calculations.

A qualitative comparison of the beryllium data is made with the lattice vibration data for zinc[19] (also hexagonal closed-packed structure) which were obtained by Joynson from x-ray measurements.

II. LATTICE DYNAMICS

Beryllium possesses the hexagonal close-packed structure which is based on the hexagonal lattice with a basis of two atoms per lattice point, one atom positioned at the lattice point and the other removed a distance

$$\mathbf{r}=\tfrac{1}{3}\mathbf{a}_1+\tfrac{2}{3}\mathbf{a}_2+\tfrac{1}{2}\mathbf{a}_3, \tag{3}$$

where $\mathbf{a}_1$, $\mathbf{a}_2$ and $\mathbf{a}_3$ are the primitive lattice basis vectors illustrated in Fig. 1(a). Values of the lattice parameters[17] are $|\mathbf{a}_1|=|\mathbf{a}_2|=a=2.2856$ Å, $|\mathbf{a}_3|=c=3.5832$ Å. As noted previously, the primitive hexagonal unit cell of beryllium contains two atoms and hence there are six branches for the dispersion relation, three acoustical and three optical.

The reciprocal lattice of beryllium is also hexagonal, as shown in Fig. 1(b), and experimental conditions were arranged such that only phonons having their wave vectors in the plane of $\mathbf{b}_2$ and $\mathbf{b}_3$ ($h=0$) were investigated. From the symmetry of beryllium (space group D_{6h}^4) it is noted that a sixfold rotation inversion axis is oriented parallel to $\mathbf{b}_3$, and a twofold axis is oriented parallel to $\mathbf{b}_2$ with another twofold axis perpendicular to $\mathbf{b}_2$ and $\mathbf{b}_3$. In addition there are mirror planes parallel to the plane of $\mathbf{b}_1$ and $\mathbf{b}_2$ and to the plane of $\mathbf{b}_2$ and $\mathbf{b}_3$. With these symmetry properties the polarization vectors ξ of waves traveling in the symmetry directions are as follows: for waves traveling in the direction of $\mathbf{b}_3$ longitudinal wave polarization is parallel to $\mathbf{b}_3$ and transverse wave polarization is in the mirror plane perpendicular to $\mathbf{b}_3$ and independent of orientation within the plane since the transverse modes are degenerate; for waves traveling in the direction of $\mathbf{b}_2$ longitudinal wave polarization is parallel to $\mathbf{b}_2$ and transverse polarizations are perpendicular to $\mathbf{b}_2$ and either parallel or perpendicular to $\mathbf{b}_3$. In crystallographic notation the directions of $\mathbf{b}_2$ and $\mathbf{b}_3$ are referred to as $[01\bar{1}0]$ and [0001], respectively.

A general model for the lattice dynamics of hexagonal close-packed metals has been developed by Slutsky and Garland. The model assumes central-force interactions with first, second, and third nearest neighbors. In accord with the symmetry cited above the 6×6 dynamical matrix $D(\mathbf{q})$, which appears in the secular equation

$$|D(\mathbf{q})-4\pi^2m\nu^2I|=0, \tag{4}$$

reduces for the [0001] direction to three 2×2 matrices: one 2×2 matrix for the longitudinal vibrations and two identical 2×2 matrices describing the transverse vibrations. For the $[01\bar{1}0]$ direction of wave propagation, the 6×6 dynamical matrix reduces to three distinct 2×2 matrices, one for longitudinal vibrations and two for transverse vibrations having their polarizations perpendicular to each other and in mirror planes. For the $[01\bar{1}0]$ direction, the transverse modes are designated $T(\|)$ and $T(\perp)$ depending on the polarization being either parallel or perpendicular to the [0001] direction. Of interest is the fact that this model predicts the presence of optical branches which do not have a common frequency for zero value of the wave vector. In addition, the identification of the upper and lower optical branches changes in going from the [0001] direction to the $[01\bar{1}0]$ direction. The upper optical branches, for the symmetry directions of interest, correspond to the modes of vibration having their polarization vectors in the [0001] direction.

With the simplification of the dynamical matrix to three 2×2 matrices for the symmetry directions the eigenfrequencies of the SG model are given by equations of the form

$$4\pi^2m\nu_j=Y_j+Z_j(\mathbf{q},11)\pm|Z_j(\mathbf{q},12)|. \tag{5}$$

Y_j is a linear combination of the force constants, $Z_j(\mathbf{q},11)$ is a real function of the wave vector and force constants of atoms on the same sublattice and $Z_j(\mathbf{q},12)$ is a complex function of the wave vector and force constants for the interaction between atoms on different

[19] R. E. Joynson, Phys. Rev. 94, 851 (1954).

sublattices. Equation (5) is identical in form to Eq. (7) of Brockhouse and Iyengar[10] for germanium. Following their assumptions and allowing for the difference in crystal structure the structure factor g_j^2 is given by

$$g_j^2=\frac{b^2(\xi_j\cdot\mathbf{Q})^2}{2m\nu_j}\left|\pm\frac{Z_j(\mathbf{q},12)}{|Z_j(\mathbf{q},12)|}+\exp(i\mathbf{Q}\cdot\mathbf{r})\right|^2, \quad (6)$$

where b is the bound atom coherent scattering length, ξ_j is the phonon polarization vector describing the direction of atom displacement for the jth mode, $\mathbf{Q}$ is defined in Eq. (1), and $\mathbf{r}$ is defined in Eq. (3). In evaluating the structure factor, the SG model has been applied with the values $\alpha=1.83$, $\beta=3.76$, and $\gamma=0$, all in units of 10^4 dyn cm^{-1}, assigned to the force constants in the notation of Slutsky and Garland. The final values assigned to α, β, and γ were determined from a least-squares fit of the SG model to the neutron data for the optical branches (preliminary evaluation of α, β, γ, and g_j^2 was made from elastic constants data). Results of the g_j^2 calculation are displayed in Fig. 2 for the symmetry directions [0001] and [01$\bar{1}$0]. The plots of g^2 labeled TA and UO for the [01$\bar{1}$0] direction refer to the transverse modes having their polarization vectors parallel to the [0001] direction (the other transverse modes for this direction were not investigated). The structure factor was used to predict the regions of reciprocal space where maximum intensity might be expected. In Fig. 3 is displayed, by bold outline, the periodic range of g_j^2 for the $h=0$ plane of reciprocal space, and for comparison the Brillouin zone or periodic range of $\nu(\mathbf{q})$ is shown in light outline.

Experimental values of the elastic constants which were used in evaluating the model of SG and in determining the initial slopes of the acoustical branches are due to Smith and Arbogast. Values of the elastic constants, in units of 10^{12} dyn cm^{-2}, are as follows: $C_{11}=2.923$; $C_{33}=3.364$; $C_{44}=1.625$; $C_{12}=0.267$; $C_{13}=0.14$.

A complicating factor which arises in the study of a solid such as beryllium stems from the fact that it is a

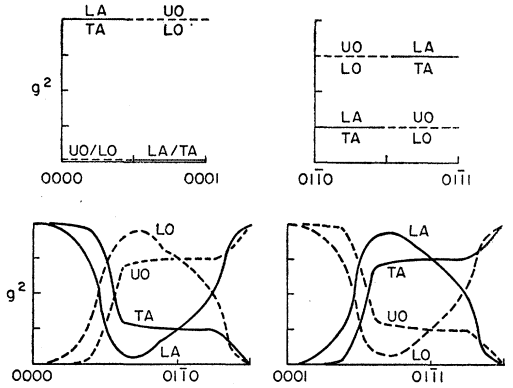

FIG. 2. Calculated structure factor g_j^2, based on the lattice dynamics model of Slutsky and Garland ($\alpha=1.83\times10^4$ dyn cm^{-1}, $\beta=3.76\times10^4$ dyn cm^{-1}, $\gamma=0$) in units of $(b\mathbf{Q}\cdot\xi)^2/2m\nu$.

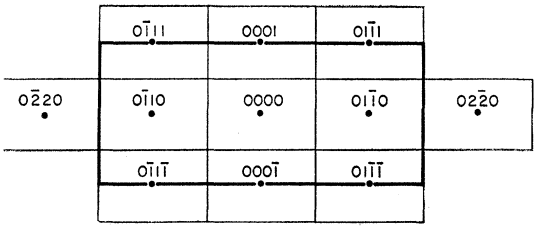

FIG. 3. The $h=0$ plane of reciprocal space showing the periodic range of the structure factor in bold outline and, for comparison, the Brillouin zone in light outline.

good neutron monochromator. In such materials it is possible that phonon scattering may be preceded by Bragg scattering[20] or followed by Bragg scattering. While analysis of the data from double scattering events of this type lead to frequency and wave vector values which are consistent with other dispersion curve data, the data do not appear to satisfy the identification of the mode of vibration in terms of the polarization factor $(\mathbf{Q}\cdot\xi)^2$ which occurs in the structure factor g_j^2. For scattering events of this type the wave vector relation in Eq. (1) should be replaced with

$$\mathbf{k}_0-\mathbf{k}''=2\pi(\tau_1+\tau_2)-\mathbf{q}. \quad (7)$$

Equation (7) is obtained by adding together the wave vector equations (1) for two successive scattering events in one of which Bragg scattering occurs ($\mathbf{q}=0$). The symbol $\mathbf{k}''$ refers to the neutron wave vector after the second scattering process, and the reciprocal lattice vectors τ_1 and τ_2 refer to the individual scattering processes.

III. EXPERIMENTAL DETAILS

The data were obtained using the MTR (Materials Testing Reactor) phased-chopper velocity selector[1], and time-of-flight methods. Chopper inserts having a radius of curvature of 83.3 in. were used with a chopper speed of 4950 rpm. The beryllium single crystal was placed in the usual sample position, $\frac{1}{2}$ m from the second chopper. Initially a total of twelve BF_3 detectors having a diameter of 1 in. and an active length of 4 in. were placed side by side with their center wires perpendicular to the scattering plane and at a distance of approximately 1.8 m from the beryllium crystal. The individual detectors were not all at exactly the same distance from the sample. Detector pulses were stored in separate sections of the 4096 channel time-of-flight analyzer for individual detectors or for sets of two detectors in parallel, thus defining from 6 to 12 closely spaced scattering angles. The group of detectors was centered on a scattering angle of 90°. During the progress of the experiment ten additional detectors were installed, the second group of detectors being centered at a scattering angle of 75° and connected in

[20] B. N. Brockhouse, T. Arase, G. Caglioti, M. Sakamoto, R. N. Sinclair, and A. D. B. Woods, Chalk River Report CRNP-946, AECL-1074 (unpublished).

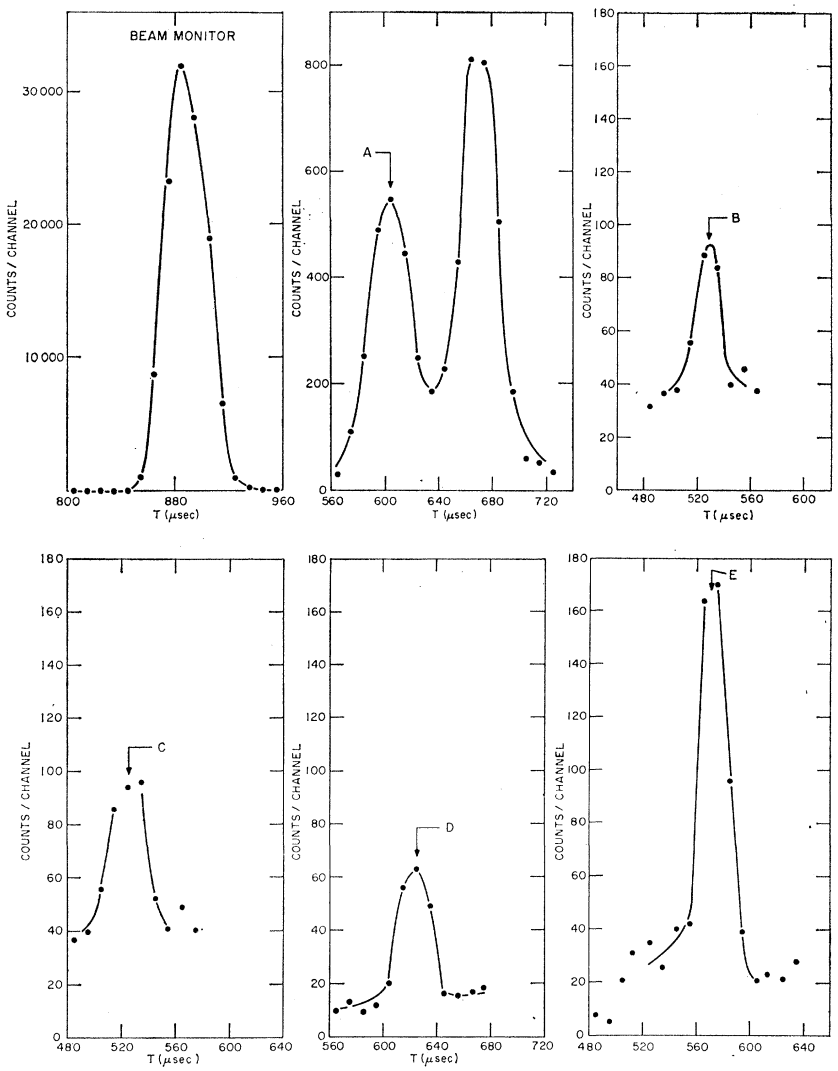

FIG. 4. Typical data obtained from 16-h runs. Initial and final neutron energies, E_0 and E, are determined from the location in the time spectrum of the centers of the data peaks of the beam monitor and scattering detectors, respectively. The letter identification of the scattering peaks can be traced to Fig. 6 and their locations on the dispersion curves.

the same manner as the original group of detectors. A fission chamber was placed in the beam path at a distance of 2.5 m from the second chopper, and data from this detector were used to determine the initial energy in a scattering experiment as well as to monitor the phase relation between choppers. It was most convenient to vary the initial energy E_0 and crystal orientation and maintain fixed scattering angles (detector positions) throughout the experiment.

The crystal was mounted on a rotary table with one of the "a" axes of the hexagonal plane in a vertical position, perpendicular to the table surface and the scattering plane of the experiment. Crystal orientation was changed during the experiment by rotation about this particular a axis. If we identify the rotation axis as $\mathbf{a}_1$, then the vectors $\mathbf{b}_2$ and $\mathbf{b}_3$ of the reciprocal lattice are normal to the axis of rotation and lie in the scattering plane [see Fig. 1(b)]. Crystal alignment was checked several times during the course of the experiment by observing Bragg reflection of neutrons from various selected crystal planes. These observations were made by using a single BF_3 detector which defined the scattering angle to within $\pm 23'$ of arc. Calibrations on the rotary table permitted the adjustment of crystal orientation to within 3′ of arc.

Dimensions of the beryllium crystal are 1.72 in. wide by 7 in. long with a thickness which tapered from 1.08 to 0.47 in. Only a portion of the crystal was exposed to the incident beam in the scattering experiment, the thickness of this portion varying from 0.64 to 1 in. One of the a-axes was approximately parallel to the 7-in. dimension of the crystal and this particular a-axis was aligned with the rotation axis of the rotary table. The angular resolution of the initial beam is $\pm 0.3°$ in the horizontal (scattering) plane and $\pm 0.8°$ in the vertical plane as determined by the size of the chopper inserts and collimation in the beam hole plug. The angle subtended by the BF_3 detectors gives an angular resolution

for the scattered neutrons of $\pm 0.4°$ in the horizontal plane for a single counter and $\pm 3.25°$ in the vertical plane.

For the time-of-flight measurements 10 μsec channel widths were used throughout the experiment. Since the time width of the monitor peak remained nearly constant, the time resolution of the incident neutrons varied in the experiment as the initial energy was varied due to the change in time-of-flight. For an incident energy of 0.025 eV the observed time resolution of the unscattered beam was $\simeq 3\%$. Minimum and maximum initial energies used were 0.013 and 0.0560 eV.

In Fig. 4 are displayed a beam monitor peak and several phonon peaks from the scattering data. These peaks are the raw data as read directly from the time-of-flight analyzer. A comparison of counting rates may be obtained as these data peaks are all for a counting time of 16 h. The letter identification of these peaks is carried over to the dispersion curves in Fig. 6 from which the phonon frequencies may be obtained. Data runs of 6 to 8 h duration were made during the day in trying to observe low-frequency states where intensities were higher, while longer runs were made over night for the higher frequency points.

The general approach to the experimental investigation was similar to the method of "successive approximations" [10] which is used with triple axis spectrometers. An estimate of the dispersion relation in a symmetry direction was made and the experimental parameters (incident neutron energy and crystal orientation) were adjusted for the 90° detector to confirm a point on the dispersion curve. These estimates were made on the basis of calculations from Eqs. (1) for the assumed values of ν and $\mathbf{q}$ and a given point in reciprocal space chosen to maximize the structure factor g_j^2 of Fig. 2 and the polarization factor $(\mathbf{Q}\cdot\boldsymbol{\xi})^2$. Quite often the estimate is wrong, the observed data do not plot in the desired symmetry direction and in the method of "successive approximations" a new estimate is made, based on the information obtained from the preceding determination. With a group of closely spaced detectors, as in this experiment, an inelastic scattering peak with a given energy change which is observed in one detector is often observed with nearly the same energy change in other detectors. These data, when plotted in reciprocal space, define scattering surfaces.[4,5,21,22] Where a scattering surface intersects a symmetry direction one can obtain a data point by calculation for the point of intersection by applying Eq. (1). Hence, while one does not always realize the aim of observing neutron interactions with phonons which are traveling in some particular crystallographic direction, the desired data are often obtained by interpolation from scattering surfaces. This technique for obtaining phonon data is

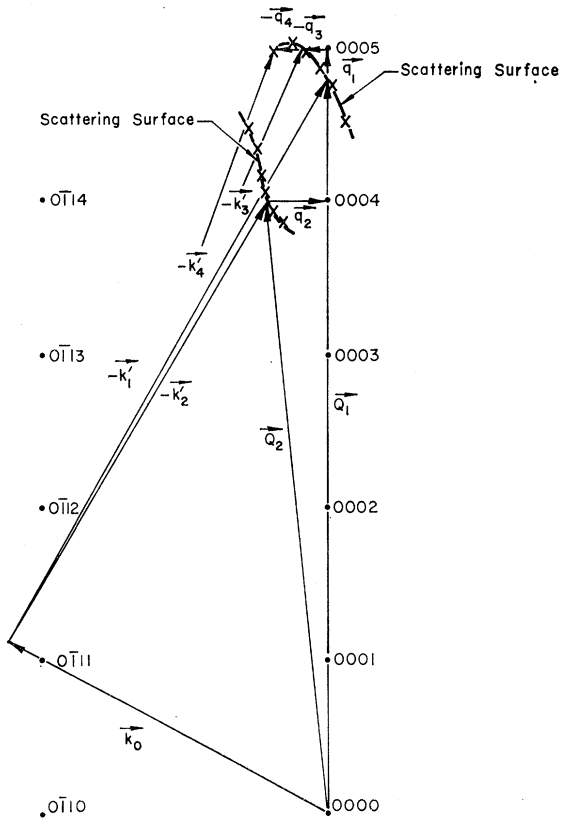

FIG. 5. Reciprocal space plot, in the plane $h=0$, of beryllium phonon data showing scattering surfaces. Actual data points are indicated by ×'s and phonon data for the symmetry directions can be obtained by interpolation from points where the scattering surfaces intercept symmetry directions, as noted by the wave vector diagrams.

referred to as the scattering surface method.[23] A typical scattering surface is displayed in Fig. 5.

Experimental data for the symmetry directions [0001] and [01$\bar{1}$0] are displayed in Fig. 6. Solid points indicate data obtained from the scattering surface method, and open points are for data obtained directly which have their wave vectors within $\pm 5°$ of the desired directions. The straight lines through the origin are the initial slopes of the acoustical branches as determined from the elastic constant data of Smith and Arbogast, and the smooth curves were hand drawn through the data. To avoid confusion in reference to the optical branches, they are referred to as upper optical (UO) and lower optical (LO). From symmetry considerations, the transverse branches are expected to be degenerate for the [0001] direction but not for the [01$\bar{1}$0] direction. The data for the [01$\bar{1}$0] direction in Fig. 6 include the transverse branches (UO) and lower frequency acoustical) which have their polarization vectors parallel to $\mathbf{b}_3$. The transverse branches in the [01$\bar{1}$0] direction, having their polarization perpendicular to the plane of

[21] G. Placzek and L. Van Hove, Phys. Rev. **93**, 1207 (1954).
[22] B. N. Brockhouse, Chalk River Report CRNP-947, AECL-1183 (unpublished).
[23] R. E. Schmunk and R. M. Brugger, Nuclear Instr. and Methods **12**, 365 (1961).

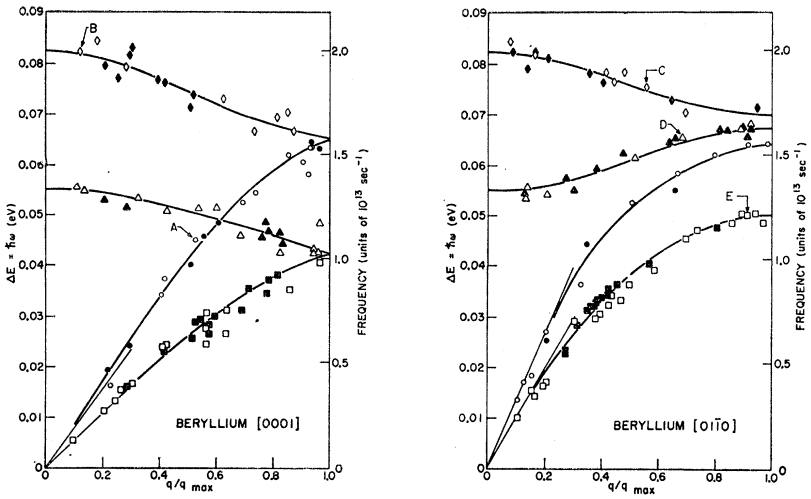

FIG. 6. Beryllium dispersion relation for the symmetry directions [0001] and [01$\bar{1}$0]. Open points refer to experimental data which plot with the phonon wave vector within ±5° of the desired direction and solid points refer to data obtained from the scattering surface method. The character of the data is as follows: ◇, upper optical; △, lower optical; ○, longitudinal acoustical; □, transverse acoustical. The smooth curves were hand drawn through the data, and the straight lines at the origin indicate the initial slopes of the acoustical branches predicted from elastic constant data. For the direction [01$\bar{1}$0], phonon polarization for the transverse acoustical and upper optical branches is parallel to [0001].

$\mathbf{b}_2$ and $\mathbf{b}_3$ and hence perpendicular to the scattering plane of the experiment could not be observed without remounting the crystal in a different orientation (i.e., $\mathbf{Q}\cdot\boldsymbol{\xi}=0$ for these branches throughout the experiment).

In mapping the different branches of the dispersion relation, the structure factor g_j^2 was followed as much as possible in determining the areas of reciprocal space in which to work, and every effort was made to maximize the polarization factor $(\mathbf{Q}\cdot\boldsymbol{\xi})^2$. The general areas of reciprocal space in which the investigations were carried out are given in Table I. The longitudinal acoustical and lower optical branches which cross for $\mathbf{q}$ in the [0001] direction were investigated in different areas of reciprocal space such that the polarization factor of the branch being investigated was maximized and the same factor for the other branch was nearly zero.

IV. DISCUSSION

In agreement with the SG and BB lattice dynamics models the experimental data indicate that for both symmetry directions, [0001] and [01$\bar{1}$0], the higher frequency optical branch corresponds to the mode of vibration having its polarization vector parallel to the hexagonal axis. Whether or not there exists a splitting of the optical and acoustical branches at the zone boundary in the [0001] direction cannot be determined from the present data. Further, there does not appear to be any question regarding the crossing of the lower optical and longitudinal acoustical branches in the [0001] direction. These two branches were investigated in different areas of reciprocal space such that the polarization factor $(\mathbf{Q}\cdot\boldsymbol{\xi})^2$ for one branch was maximized and simultaneously the polarization factor for the other branch was nearly zero. In this way each of the two branches was investigated individually without the presence of interference from the other branch.

TABLE I. Regions of reciprocal space in which the specified branches of the dispersion relation were investigated.

Branch \ Direction	[0001]	[01$\bar{1}$0]
Transverse acoustical	between (0,2,$\bar{2}$,1) and (0,2,$\bar{2}$,0.5)	between (0,0,0,4) and (0, 0.5, −0.5, 4)
Longitudinal Acoustical	near (0,0,0,4)[a]	near (0,2,2,0)[a] and between (0,2,$\bar{2}$,1) and (0, 2.5, −2.5, 1)
Lower optical	between (0,2,$\bar{2}$,0) and (0, 2.5, −2.5, 0.5)	between (0,2,$\bar{2}$,0) and (0, 2.5, −2.5, 0)
Upper optical	near (0,0,0,5)[a]	between (0,0,0,5) and (0, 0.5, −0.5, 5)

[a] On a line connecting the specified reciprocal lattice point with the origin.

For the acoustical branches displayed in Fig. 6 the experimental data join smoothly to the initial slopes predicted from elastic constant data for three of the four branches. In the case of the fourth acoustical branch, LA[0001], the data points lie above the initial slope line for half the wave vector range in the Brillouin zone. Although the data in the region of small values of $\mathbf{q}$ are not sufficient to show that the curve has the correct slope at $\mathbf{q}=0$ the data for larger values of $\mathbf{q}$ do suggest the presence of long-range forces in the crystal. Further inspection of the acoustical branches indicates that the Debye approximation is reasonable for the [0001] direction but not for the [01$\bar{1}$0] direction where the dispersion is more pronounced.

Comparison of lattice dynamics models with the experimental data can be made by solving the dynamical equations for phonon wave vectors in the directions of interest, [0001] and [01$\bar{1}$0]. A plot of the solution in the form $\nu(\mathbf{q})$ vs $q/q_{\max}$ gives a direct comparison with the experimental data.

Slutsky and Garland Model

Qualitatively, the SG model is in agreement with experimental data. In particular, the general separation of the optical branches and the crossing of the lower optical branch and the longitudinal acoustical branch in the [0001] direction are both predicted by the model as well as the over-all general shape of the dispersion

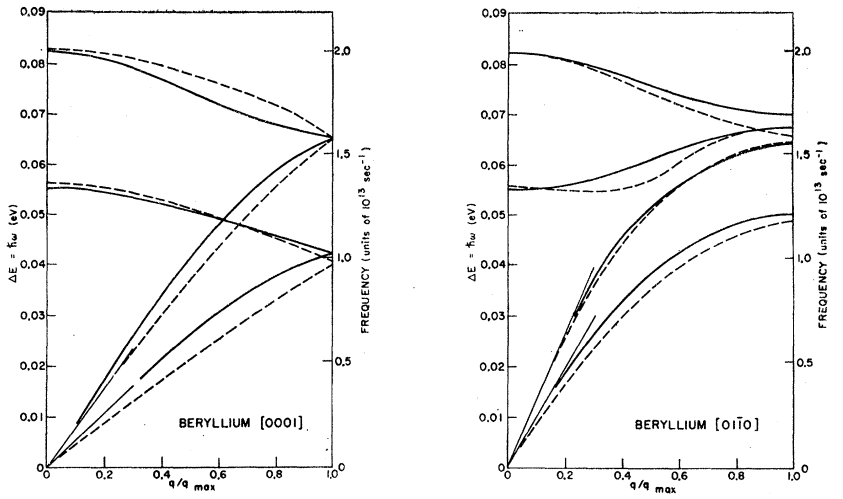

FIG. 7. The dashed curves are for the extended model of Slutsky and Garland fitted to the neutron scattering data and compared to the smooth curves of Fig. 6 which were hand drawn through the experimental data.

curves for both symmetry directions. Further, it is concluded that the structure factor g_j^2 which was calculated from the SG model is a good approximation to the real quantity.

Quantitatively, however, the SG model is inadequate when the force constants are evaluated from the elastic constants. This statement is based on comparison of the model with experiment for the optical intercepts at the center of the Brillouin zone, the initial slopes of the acoustical branches, and the frequency ranges of both acoustical and optical branches.

In the SG model, central forces are assumed with the further simplification that only terms quadratic in the displacements of the atoms from their equilibrium positions are retained in the expression for the potential energy, and that derivatives of the potential energy are evaluated about the potential minimum. Thus, there are three force constants (for describing the interaction of a given atom with first, second, and third nearest neighbors) plus a volume-dependent electron gas constant σ which are related to the five independent elastic constants. The problem of evaluating the four unknown constants in terms of the elastic constants is over determined and the values obtained for the force constants when introduced into the dynamic equations of motion yield results which are not consistent with the experimental data. For example, the upper optical branch is predicted to have an intercept at the center of the Brillouin zone of 2.9×10^{13} sec^{-1} compared to the experimental value of $1.99\pm0.07\times10^{13}$ sec^{-1}.

An alternative method of evaluating the force constants is provided by the fact that for certain points in the Brillouin zone the eigenvalues $(4\pi^2m\nu^2)$ in the secular equation are given directly by a linear combination of the force constants. Introducing the experimentally observed eigenvalues into the equations for these points the dynamic equations can be fit directly to the experimental data. Points in the Brillouin zone for which this simplification of the dynamic equations exists are the center of the zone and at the zone boundaries in both [0001] and [01$\bar{1}$0] directions.

Evaluation of the SG model in the manner just described is still unsatisfactory. In an effort to improve the fit of this model to the experimental data, the SG model has been extended to include interactions with fourth and fifth nearest neighbors and is, hereafter, referred to as the extended SG model. The general formulation of this calculation, which is applicable to other hexagonal close-packed metals, is included in the Appendix. The force constants in the extended SG model have been evaluated in terms of the experimental data. The linear force constant relations which result from the simplification of the lattice dynamic equations at the specified points in the Brillouin zone are listed in Table II. Values of the force constants for the extended SG model which were obtained from a least-squares solution of the relations of Table II are, in units of 10^4 dyn cm^{-1}: $\alpha=1.60$, $\beta=2.66$, $\gamma=0.188$, $\delta=0.668$, and $\epsilon=0.454$.

The extended SG model, fitted to the experimental data, and displayed as the dashed lines in Fig. 7 is compared to the solid lines of Fig. 6 which were hand drawn through the data points. The extended SG mode. is seen to deviate from the experimental data particularly for the [0001] acoustical branches and the [01$\bar{1}$0] lower optical branch. For both the SG model and the extended SG model the lower optical and transverse acoustical branches for the [0001] direction can be considered as a sine curve folded back at $q/q_{\max}=1$. Thus, in fitting the models to the experimental data one has the choice of setting the amplitude of the sine curve to fit the lower optical branch or the initial slope to fit the acoustical branch, but not both. A compromise set of values would not fit either optical or acoustical branch adequately.

It is interesting to compare the value of the force constant α for interactions with nearest neighbors in the hexagonal plane with the force constant β for the

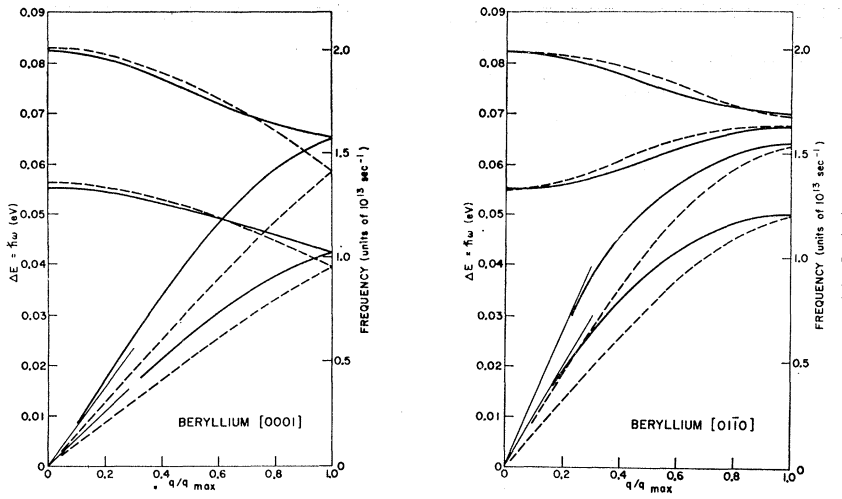

FIG. 8. The dashed curves are for the model of Begbie and Born fitted to the neutron scattering data and compared to the smooth curves of Fig. 6 which were hand drawn through the experimental data.

interactions with nearest neighbors out of the hexagonal plane. In both the SG model and the extended SG model, β is considerably larger than α even though the distances from the reference atom differ by less than 3%. This asymmetry of the interatomic forces presumably plays an important role in the separation of the optical branches, a phenomenon which is not observed for monatomic cubic crystals. Further, this asymmetry suggests that there may be interactions with more distant neighbors which are important, where the forces are directed approximately along the hexagonal axis. The experimental data for the LA[0001] branch indicate that either a more general type of force is needed to describe the dynamics of atomic motion in the solid or that forces of long range are not taken adequately into account in the model. The latter would appear to be the case because of the lack of character predicted by the BB model which is discussed next.

Begbie and Born Model

The BB model was developed without any assumptions as to the nature of the interatomic forces, assuming only that these forces are restricted to interactions with nearest neighbors in and out of the hexagonal plane. There are eight force constants in the model and not all of these can be evaluated from elastic constant data. Those force constants[24] which can be evaluated give predicted optical intercepts at the center of the Brillouin zone of 2.40 and 1.65, in units of 10^{13} sec^{-1}, values which are approximately 20% higher than the observed values. The alternative of evaluating the force constants in terms of the experimental data has been applied as in the SG model and the extended SG model. In Table III are listed the linear force constant relations obtained from the dynamic equations of the BB model for the specified branches and directions. Values obtained for the force constants in this model are, in the notation of Begbie and Born and in units of 10^4 dyn cm^{-1}: $\nu=1.95$; $\lambda=0.871$; $\gamma=0.145$; $(\alpha+\beta)=1.21$; and $\mu=0.118$. Measurements of phonons with their wave vectors in the [01$\bar{1}$0] direction and their polarization vectors parallel to the basal plane would enable one to determine individual values for the constants α and β. However, one of the force constants, δ, cannot be evaluated from phonon data for the symmetry directions. In Fig. 8 the BB model is displayed as the dashed lines and compared to the experimental data which are represented by the solid lines. The BB model gives a reasonable fit to the optical branches but is consistently low for all of the acoustical branches and does not describe the dispersion present in the acoustical branches. The model is expected to fit better for the optical branches for it is the data from these branches which have been used predominantly in evaluating the force constants in the model. Evaluating the force constants to fit the acoustical branches would give the same result as evaluating the force constants in terms of the elastic constants data. Because of the general nature of the forces in this model it is desirable to extend the model to include interactions with more

TABLE II. Observed frequencies and force constants relations for the specified branches and points in the Brillouin zone which were used to evaluate the force constants in the extended Slutsky and Garland model.

Designation	Observed frequencies ν (10^{13} sec^{-1})	Force constant relations for the extended SG model $4\pi^2 m\nu^2$
UO($q=0$)	1.99	$(3c/a)^2(\beta'+\gamma'/4+2\epsilon'/7)$
LO($q=0$)	1.33	$6(\beta+\gamma'+2\epsilon')$
UO[01$\bar{1}$0]$q=q_{\max}$	1.69	$(3c/a)^2(2\beta'/3+4\epsilon'/21)$
LO[0110]$q=q_{\max}$	1.63	$2(3\alpha+2\beta'+3\gamma'+16\epsilon'/7)$
LA[01$\bar{1}$0]$q=q_{\max}$	1.54	$2(3\alpha+\beta'+26\epsilon'/7)$
TA[01$\bar{1}$0]$q=q_{\max}$	1.22	$(3c/a)^2(\beta'/3+\gamma'/4+2\epsilon'/21)$

[24] A systematic error of $8\pi^2$ appears in the equation of Begbie and Born relating the elastic constants to the force constants of their model. The correct equations are given in the paper by Joynson, reference 19 of this paper.

distant neighbors. However, extension of the model would be considerably more difficult than extension of the SG model. Collins[25] has combined the SG and BB models in attempting to fit experimental data for magnesium, using the BB model and general forces for first and second nearest-neighbor interactions and the SG model and central forces for treating interactions with more distant neighbors. Although no indication of the success of Collins' fitting has been received, his approach appears worthy of consideration in attempting to fit the beryllium data.

X-Ray Measurements on Zinc

The present measurements can be compared qualitatively with x-ray measurements of the phonon dispersion relation of zinc, which also has the hexagonal close-packed structure. The measurements on zinc were made by Joynson using the BB model as a guide. For those branches of the dispersion relation which were measured in both the zinc experiment and the present experiment the general shape of the curves is approximately the same and that is all that one might expect. Of importance is the fact that the optical frequencies observed in the zinc experiment ($\mathbf{q}=0$) are not consistent for the two symmetry directions. The optical branches labeled longitudinal and transverse t_1 for the direction $\mathbf{b}_2$ in the zinc experiment should have the same intercept frequency at the center of the Brillouin zone (lower optical) as the transverse optical branch for the direction $\mathbf{b}_3$. This result is predicted by both BB and SG models and verified in the case of beryllium by the present measurements. The discrepancies in the x-ray data are considered as further support of the superiority of neutron scattering methods.

V. SUMMARY

The experimental data obtained for the phonon dispersion relation of beryllium provide a contrast to the data obtained from the investigation of cubic metals. The asymmetry of the force field in hexagonal close-packed beryllium is indicated in the separation of the optical branches for zero value of the wave vector. Lattice dynamics models of Begbie and Born and of Slutsky and Garland, the latter model extended in the present investigation, give limited agreement with the experimental data only when the force constants in the models are evaluated directly from the phonon data. Although the agreement between the models and the experimental data is considered adequate to use the models for calculating properties involving the frequency distribution, a better model appears to be one which combines the two models, allowing for general forces between near neighbors and central-force interactions with more distant neighbors.

TABLE III. Observed frequencies and force constants relations for the specified branches and points in the Brillouin zone which were used to evaluate the force constants in the Begbie and Born model.

Designation	Observed frequencies ν (10^{13} sec^{-1})	Force constant relation $4\pi^2 m\nu^2$
UO($q=0$	1.99	12ν
LO($q=0$)	1.33	12λ
UO[$01\bar{1}0$]$q=q_{\max}$	1.69	$8(\nu+\gamma)$
LO[$01\bar{1}0$]$q=q_{\max}$	1.63	$8(\lambda+\alpha+\beta+\mu)$
LA[$01\bar{1}0$]$q=q_{\max}$	1.54	$4[\lambda+2(\alpha+\beta-\mu)]$
TA[$01\bar{1}0$]$q=q_{\max}$	1.22	$4(\nu+2\gamma)$

[25] G. L. Squires (private communication).

ACKNOWLEDGMENTS

The authors would like to acknowledge the assistance of Mrs. Carolyn Slayden with computations; Norman Tolk and Robert Henscheid, summer students who worked on the experiment; Dr. R. C. Young for checking Eqs. (8) in the Appendix; and Dr. J. E. Evans and Dr. R. G. Fluharty for their continued support.

APPENDIX

In the following paragraphs results are stated for the extension of the Slutsky and Garland model of the lattice dynamics of hexagonal close-packed metals to include interactions with fourth and fifth nearest neighbors. Also, it should be noted that corrections are included for certain of the terms involving the third neighbor constant γ (or γ'), which were incorrectly stated in the original paper. The notation of Slutsky and Garland is continued in the extended model.

The hexagonal close-packed structure can be considered as two interpenetrating hexagonal lattices, the basis translation vectors of which are defined relative to an orthogonal coordinate system as $\mathbf{a}_1=a(1,0,0)$, $\mathbf{a}_2=a(-1/2,\sqrt{3}/2,0)$ and $\mathbf{a}_3=c(0,0,1)$. The position vector of an arbitrary atom in the structure is given by $\mathbf{r}(l,j)=\mathbf{r}(l)+\mathbf{r}(j)$, where $\mathbf{r}(l)=\sum_i l_i\mathbf{a}_i$ is a lattice translation vector and $\mathbf{r}(j)$ locates the atom on one or another of the two interpenetrating lattices. One of the lattices has $\mathbf{r}(j=1)=0$ and the other has $\mathbf{r}(j=2)=(\mathbf{a}_1/3)+(2\mathbf{a}_2/3)+(\mathbf{a}_3/2)$. There are two fourth nearest neighbors at a distance c from the reference atom which interact with the force constant δ, and twelve fifth nearest neighbors which are at a distance $[(c/2)^2+7a^2/3]^{1/2}$ and interact with force constant ϵ. The fourth nearest neighbors are along the hexagonal axis above and below the reference atom. In Table IV are listed the additional neighbors for the two atoms in the primitive hexagonal unit cell: Unprimed numbers refer to the neighbors of the atom at the origin, $\mathbf{r}(l=0,\ j=1)$, and primed numbers refer to the neighbors of the atom at the position $\mathbf{r}(l=0,\ j=2)$. Positions of the first, second, and third nearest neighbors were given in the work of Slutsky and Garland.

The lattice contribution to the elastic constants has

been calculated using the method of homogeneous deformation as in the original model. Relations between the force constants and elastic constants are as follows:

$$C_{11}=\frac{1}{2\sqrt{3}c}\Big[3(3\alpha+\beta'+4\gamma'+14\epsilon')-\frac{[\beta'-2\gamma'+(20/7)\epsilon']^2}{(\beta'+\gamma'+2\epsilon')}\Big]+\sigma,$$

$$C_{12}=\frac{1}{2\sqrt{3}c}\Big[3\alpha+\beta'+4\gamma'+14\epsilon'+\frac{[\beta'-2\gamma'+(20/7)\epsilon']^2}{(\beta'+\gamma'+2\epsilon')}\Big]+\sigma,$$

$$C_{33}=(\sqrt{3}c/a^2)[\beta\sin^2\psi+\gamma\sin^2\theta+\tfrac{4}{3}\delta+(3/14)(c/a)^2\epsilon']+\sigma,$$

$$C_{44}=(\sqrt{3}c/2a^2)(\beta'+\gamma'+2\epsilon'),$$

$$C_{13}=C_{44}+\sigma. \tag{8}$$

The force constant ϵ has been replaced with ϵ' in Eq. (8) where $\epsilon'=\epsilon\cos^2\Phi$ and $\cos^2\Phi=7a^2/(3c^2/4+7a^2)$.

Contributions of the additional force interactions to the dynamic equations of motion are viewed in the secular Eq. (4) which is given in Sec. II.

TABLE IV. Positions of fourth and fifth neighbors of atoms O and O'.

Atom	j	l_1	l_2	l_3	Atom	j	l_1	l_2	l_3
19, 1′	1	0	0	1	19′	2	0	0	1
20	1	0	0	−1	20′, 4	2	0	0	−1
21, 8′	2	1	1	0	21′	1	−1	−1	1
22, 9′	2	0	1	0	22′	1	0	−1	1
23	2	−2	−1	0	23′	1	2	1	1
24	2	−2	−2	0	24′	1	2	2	1
25	2	0	−2	0	25′	1	2	0	1
26	2	1	−1	0	26′	1	−1	1	1
27	2	1	1	−1	27′, 11	1	−1	−1	0
28	2	0	1	−1	28′, 12	1	0	−1	0
29	2	−2	−1	−1	29	1	2	1	0
30	2	−2	−2	−1	30′	1	2	2	0
31	2	0	−2	−1	31′	1	2	0	0
32	2	1	−1	−1	32′	1	−1	1	0

In Eq. (4), I is the unit matrix and $D(\mathbf{k})$,[26] a function of the wave vector $\mathbf{k}$, is a 6×6 matrix which is related to 3×3 submatrices A and B by the relation

$$D(k)=\begin{bmatrix}A & B\\ B^* & A\end{bmatrix},$$

and B^* is the complex conjugate of B. With the additional interactions considered, the elements of A and B are

$$A_{11}=\alpha[3-2C_1-\tfrac{1}{2}(C_{12}+C_2)]+3\beta'+3\gamma'+6\epsilon',$$

$$A_{22}=3\alpha[1-\tfrac{1}{2}(C_{12}+C_2)]+3(\beta'+\gamma'+2\epsilon'),$$

$$A_{33}=(9/2)(c/a)^2(\beta'+\tfrac{1}{4}\gamma')+2\delta(1-C_3)+(9/7)(c/a)^2\epsilon',$$

$$A_{21}=A_{12}=-\tfrac{1}{2}\sqrt{3}\alpha(C_{12}-C_2),$$

$$A_{31}=A_{32}=A_{13}=A_{23}=0,$$

$$B_{11}=-\tfrac{3}{4}[\beta'(C_2+C_{12}+C_{23}+C_{123})+2\gamma'C_1(1+C_3)]+\tfrac{3}{4}[\beta'(S_2+S_{12}+S_{23}+S_{123})+2\gamma'C_1S_3]i$$
$$-(3\epsilon'/28)\{(1+C_3)(C_2+C_{12})+S_3(S_2+S_{12})+9[C_{212}+C_{2123}+C_1(C_2+C_{23})+S_1(S_2+S_{23})]$$
$$+4(C_{2122}+C_{22}+C_{21223}+C_{223})\}-(3\epsilon'/28)i\{(1+C_3)(S_2+S_{12})-S_3(C_2+C_{12})+9[S_1(C_2+C_{23})-C_1(S_2+S_{23})$$
$$-S_{212}-S_{2123}]-4(S_{2122}+S_{22}+S_{21223}+S_{223})\},$$

$$B_{22}=-\{\beta'[1+C_3+\tfrac{1}{4}(C_2+C_{12}+C_{23}+C_{123})]+\gamma'[C_{122}+C_{1223}+\tfrac{1}{2}C_1(1+C_3)]\}+i\{\beta'[S_3+\tfrac{1}{4}(S_2+S_{12}+S_{23}+S_{123})]$$
$$+\gamma'(S_{122}+S_{1223}+\tfrac{1}{2}C_1S_3)\}-(\epsilon'/28)\{25[(1+C_3)(C_2+C_{12})+S_3(S_2+S_{12})]+C_{212}+C_{2123}+C_1(C_2+C_{23})$$
$$+S_1(S_2+S_{23})+16(C_{2122}+C_{21223}+C_{22}+C_{223})\}-(\epsilon'/28)i\{25[(S_2+S_{12})(1+C_3)-S_3(C_2+C_{12})]+S_1(C_2+C_{23})$$
$$-C_1(S_2+S_{23})-S_{212}-S_{2123}-16(S_{2122}+S_{21223}+S_{22}+S_{223})\},$$

$$B_{33}=-(3c^2/4a^2)\{\beta'(1+C_2+C_3+C_{12}+C_{23}+C_{123})+\tfrac{1}{4}\gamma'[2C_1(1+C_3)+C_{122}+C_{1223}]\}$$
$$+i(3c^2/4a^2)\{\beta'(S_3+S_2+S_{12}+S_{23}+S_{123})+\tfrac{1}{4}\gamma'(2C_1S_3+S_{122}+S_{1223})\}-\epsilon'(3c^2/28a^2)\{(1+C_3)(C_2+C_{12})$$
$$+C_1(C_2+C_{23})+S_3(S_2+S_{12})+S_1(S_{23}+S_2)+C_{212}+C_{2122}+C_{22}+C_{2123}+C_{21223}+C_{223}+i[S_1(C_2+C_{23})$$
$$+S_2(1-C_1+C_3)-S_3(C_2+C_{12}+C_{212}+C_{2122}+C_{22})-(1+C_3)(S_{212}+S_{2122}+S_{22}-S_{12})-S_{23}C_1]\},$$

$$B_{21}=B_{12}=-\tfrac{1}{4}\sqrt{3}\{\beta'(-C_2+C_{12}-C_{23}+C_{123})+2\gamma'S_1S_3+i[\beta'(S_2-S_{12}+S_{23}-S_{123})+2\gamma'S_1(1+C_3)]\}$$
$$-(\sqrt{3}/28)\epsilon'\{5[C_{12}(1+C_3)+S_3(S_{12}-S_2)-C_2(1+C_3)]+3[C_{212}+C_{2123}-C_1(C_2+C_{23})-S_1(S_2+S_{23})]$$
$$+8(C_{2122}+C_{21223}-C_{22}-C_{223})\}-(\sqrt{3}/28)\epsilon'i\{5[(1+C_3)(S_{12}-S_2)+S_3(C_2-C_{12})]$$
$$+3[C_1(S_2+S_{23})-S_1(C_2+C_{23})-S_{212}-S_{2123}]+8(S_{22}+S_{223}-S_{2122}-S_{21223})\},$$

[26] The symbol $\mathbf{q}$ which was used to designate the phonon wave vector in the main body of the paper for consistency with the reference is changed to the symbol $\mathbf{k}$ which Slutsky and Garland use in their paper.

$$B_{31}=B_{13}=-(3c/4a)\{\beta'(C_2-C_{12}-C_{23}+C_{123})-\gamma'S_1S_3-i[\beta'(S_2-S_{12}-S_{23}+S_{123})-\gamma'S_1(1-C_3)]\}$$
$$-(3c/28a)\epsilon'\{(1-C_3)(C_{12}-C_2)+S_3(S_2-S_{12})+3[C_1(C_2-C_{23})+S_1(S_2-S_{23})-C_{212}+C_{2123}]$$
$$+2(-C_{2122}+C_{21223}+C_{22}-C_{223})\}-i(3c/28a)\epsilon'\{S_3(C_{12}-C_2)+(S_{12}-S_2)(1-C_3)$$
$$+3[S_1(C_2-C_{23})+C_1(S_{23}-S_2)+S_{212}-S_{2123}]+2(S_{2122}-S_{21223}-S_{22}+S_{223})\},$$

and

$$B_{23}=B_{32}=-(\sqrt{3}c/2a)\{\beta'[1-C_3+\tfrac{1}{2}(-C_2-C_{12}+C_{23}+C_{123})]+\tfrac{1}{2}\gamma'[C_{1223}-C_{122}+C_1(1-C_3)]\}$$
$$-i(\sqrt{3}c/2a)\{\beta'[S_3+\tfrac{1}{2}(S_2+S_{12}-S_{23}-S_{123})]+\tfrac{1}{2}\gamma'(S_{122}-S_{1223}+C_1S_3)\}-\epsilon'(\sqrt{3}/28)(c/a)\{5[(1-C_3)(C_2+C_{12})$$
$$-S_3(S_2+S_{12})]+C_1(C_{23}-C_2)+S_1(S_{23}-S_2)-C_{212}+C_{2123}+4(-C_{22}+C_{223}-C_{2122}+C_{21223})\}$$
$$-i(\sqrt{3}/28)(c/a)\epsilon'\{5[(1-C_3)(S_2+S_{12})+S_3(C_2+C_{12})]+S_1(C_{23}-C_2)+C_1(S_2-S_{23})+S_{212}-S_{2123}$$
$$+4(S_{22}-S_{223}+S_{2122}-S_{21223})\}.$$

The notation

$$C_i=\cos 2\pi k_i,$$
$$C_{ij}=\cos 2\pi(k_i+k_j),$$
$$C_{122}=\cos 2\pi(k_1+2k_2),$$
$$C_{123}=\cos 2\pi(k_1+k_2+k_3),$$
$$C_{1223}=\cos 2\pi(k_1+2k_2+k_3),$$

and

$$C_{21223}=\cos 2\pi(2k_1+2k_2+k_3)$$

has been used, and the S's refer to the corresponding sines.

Corrections to the third-neighbor terms in the original model include changes of the coefficient of γ' for the elastic constant C_{44} in Eq. (8) and the coefficient of γ' in the equations for the terms A_{33}, B_{33}, B_{13}, and B_{23}.

PHYSICAL REVIEW VOLUME 128, NUMBER 2 OCTOBER 15, 1962

Charged Dislocations in Ionic Crystals*

J. S. KOEHLER, D. LANGRETH, AND B. VON TURKOVICH
Department of Physics, University of Illinois, Urbana, Illinois

(Received March 1, 1962)

The paper aims to show that the charge clouds around dislocations are important for the mechanical properties of ionic crystals. The previous work of Eshelby, Newey, Pratt, and Lidiard is extended by solving the nonlinear equation giving the potential distribution and by obtaining the boundary condition appropriate at the dislocation core. Three typical examples are worked out in detail. Finally, a series of experimental phenomena are discussed and it is shown how the charge cloud model can be used to understand the experimental behavior. In particular, the minimum in the yield stress versus annealing temperature of NaCl doped with a known concentration of $PbCl_2$ is used to obtain the energy of formation of a positive ion vacancy in NaCl. One finds that $E_F^+=0.53$ eV.

I. INTRODUCTION

IN this paper we shall try to show that the idea of charged dislocations screened by a cloud of charged lattice defects enables a number of mechanical and electrical properties of ionic crystals to be understood. This idea was first discussed by Eshelby, Newey, Pratt, and Lidiard[1] who used the theory of the charge cloud in the static case to understand the temperature dependence of the yield stress of NaCl crystals.

In Sec. II the general principles appropriate for static dislocations will be described. The equations obtained will be useful for pure and for crystals containing divalent positive impurity ions. Two essential additions to the theory will be described. First, Eshelby and co-workers simplified the problem by linearizing it. We have solved the nonlinear equations. Second, Eshelby and co-workers were not able to treat the region near the core of the dislocations; in fact, they did not establish what boundary condition the potential should satisfy at the dislocation core. We have attempted to deal with this region with considerable care. Applications of the theory to various experimental observations are described in Sec. III.

II. GENERAL THEORY FOR STATIC DISLOCATIONS

Qualitatively the charge cloud arises as follows: consider a dislocation which has some edge type character. Suppose that the energy E_F^+ required to form a posi-

* This research supported in part by the National Science Foundation.

[1] J. D. Eshelby, C. W. A. Newey, P. L. Pratt, and A. B. Lidiard, Phil. Mag. 3, 75 (1958).